

K. Karpinska,<sup>1,\*</sup> M. Mostovoy,<sup>1</sup> M.A. van der Vegte,<sup>1</sup> A. Revcolevschi,<sup>2</sup> and P.H.M. van Loosdrecht<sup>1,†</sup><sup>1</sup>*Materials Science Center, University of Groningen,  
Nijenborgh 4, 9747 AG Groningen, The Netherlands*<sup>2</sup>*Laboratoire de Physico-Chimie de l'Etat Solide, Université Paris XI, France*

(Dated: November 15, 2018)

Photoluminescence excitation spectroscopy has revealed a novel, highly efficient two-photon excitation method to produce a cold, uniformly distributed high density excitonic gas in bulk cuprous oxide. A study of the time evolution of the density, temperature and chemical potential of the exciton gas shows that the so called quantum saturation effect that prevents Bose-Einstein condensation of the ortho-exciton gas originates from an unfavorable ratio between the cooling and recombination rates. Oscillations observed in the temporal decay of the ortho-excitonic luminescence intensity are discussed in terms of polaritonic beating. We present the semiclassical description of polaritonic oscillations in linear and non-linear optical processes.

PACS numbers: 71.35.Lk, 71.36+c, 78.47.+p, 78.55.Hx

## I. INTRODUCTION

The quest for Bose-Einstein condensation (BEC) of excitons has been one of the main driving forces behind the numerous studies on high density excitonic gases during the last few decades.<sup>1,2</sup> A variety of systems have been tried, including bulk crystals<sup>2,3</sup> and quantum well systems.<sup>4,5</sup> In spite of the intense effort there still is no clear evidence that condensation was actually reached. The formation of a condensate is expected to occur if the Bose gas reaches a quasi-equilibrium state characterized by a sufficiently high density  $n$  and, simultaneously, a sufficiently low temperature  $T$ . For a three dimensional non-interacting Bose gas in equilibrium the transition temperature  $T_c$  is proportional to  $n^{2/3}$ . Strong spatial confinement and decreased dimensionality lead to a substantial decrease of the condensation temperature. This is why bulk crystals remain very attractive in the search for excitonic BEC. The long life times ( $> 1$  ns) and high binding energy (150 meV) of the excitons in  $\text{Cu}_2\text{O}$  make cuprous oxide an excellent candidate in this class. In addition, the small Bohr radius ( $a_B \approx 7 \text{ \AA}$ ) of the ground state exciton assures that even at densities as high as  $n \approx 10^{20} \text{ cm}^{-3}$  the exciton-exciton interactions remain weak.<sup>6</sup> Apart from the intriguing possibility of BEC, there is a number of other interesting phenomena and properties of the exciton gas in  $\text{Cu}_2\text{O}$  which attracted attention, including localization of excitons in a stress trap,<sup>7,8</sup> spectroscopy on intra-excitonic transitions,<sup>9</sup> and the observation of polariton beating in transmission experiments resulting from interference of excited states belonging to different polariton dispersion branches.<sup>10,11</sup> In this paper we revisit the high density ortho exciton gas in  $\text{Cu}_2\text{O}$ . The first part of the paper is concerned with spectroscopic photoluminescence excitation experiments revealing a novel and efficient non-linear exciton excitation scheme, which has several advantages over the schemes used so far. In addition, we present a study of some of the statistical properties of the thus created exciton gas, and comment on the origin of the so called “quantum saturation effect”<sup>12</sup> that prevents BEC in the ortho-exciton gas in cuprous oxide. The second part of the paper concentrates on the polaritonic beating effect observed in our experiment for which a novel analytical model will be introduced. The new model explains both the beating reported earlier<sup>10,11</sup> for the transmission geometry as well as our results obtained for the back-reflection configuration.

Cuprous oxide,  $\text{Cu}_2\text{O}$ , has four different excitonic series. These are attributed to various combinations of valence ( $V$ ) band holes and conduction ( $C$ ) band electrons (see Fig. 1):  $V_1 - C_1$  (yellow),  $V_2 - C_1$  (green),  $V_1 - C_2$  (blue) and  $V_2 - C_2$  (indigo). The two uppermost valence bands originate from  $3d$  copper orbitals (split by spin-orbit interaction) while the lowest conduction band is mainly formed from  $4s$  copper orbitals.<sup>13</sup> Hence all three bands ( $V_1$ ,  $V_2$  and  $C_1$ ) have the same even parity, and an optically forbidden direct gap ( $E_g = 2.17 \text{ eV}$  at 10 K) exists at a center of a Brillouin zone. The lowest excitonic state of the system is split by the electron-hole exchange interaction into a  $1s$ -ortho state ( $J = 1$ ) at 2.033 eV ( $X_{\text{ortho}}$ ) and a  $1s$ -para state ( $J = 0$ ) at 2.021 eV ( $X_{\text{para}}$ ). As a consequence of the even parity of the bands involved, the efficiency of “direct” optical pumping of the yellow excitons is very low. Radiative decay of  $1s$  ortho-excitons is weakly allowed through a quadrupolar coupling. For the  $1s$ -para-exciton radiative transitions are forbidden to high order.

The yellow ortho-exciton emission spectrum consists of two main features: a direct  $k \approx 0$  transition ( $X_{\text{ortho}}^{\text{DI}}$ ) at 2.034 eV, and a phonon-assisted ( $X_{\text{ortho}}^{\text{PA}}$ ) emission band at 2.02 eV (see Fig.1). The PA-band results from decay by simultaneous emission of a photon and a LO-phonon of energy 13.6 meV. Since both the matrix element and the phonon dispersion are nearly  $k$ -independent<sup>14</sup> the shape of the PA band directly reflects the kinetic energy distribution

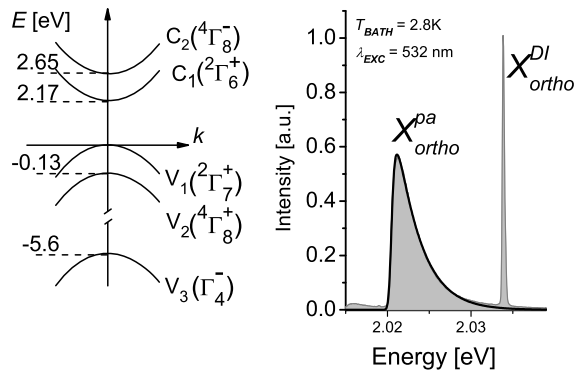


FIG. 1: Left panel: Schematic energy band diagram at the  $\Gamma$  point in  $\text{Cu}_2\text{O}$ . Right panel: Ortho-exciton emission spectrum at  $T = 2.8$  K using 532 nm continuous wave excitation. The thick line represents a fit to Eq.(1) using a Maxwell-Boltzmann distribution with  $T_{\text{be}} = 24.7$  K.

of the ortho-exciton gas. The observed emission band may therefore be described by

$$I(E) = A \int_{-\infty}^{\infty} D(x) f(x) e^{(\frac{x-E}{\Gamma})^2} dx, \quad (1)$$

where  $D(E) \propto E^{1/2}$  is the density of excitonic states (assuming a quadratic dispersion), and  $f(E)$  is either the Maxwell-Boltzmann ( $f_{\text{mb}}$ , classical gas) or Bose-Einstein ( $f_{\text{be}}$ , quantum gas) distribution function. The product  $D(x)f(x)$  is convoluted with a Gaussian experimental resolution function of width  $\Gamma$ . Fitting this equation to the experimentally observed spectrum yields an estimate for the effective excitonic temperature and chemical potential ( $\mu$ ). For an ideal Bose gas above the condensation temperature, the density of bosons is given by

$$n = g(m^*/2\pi\hbar^2)^{3/2} \int f_{\text{be}}(E, \mu, T) D(E) dE, \quad (2)$$

with  $g$  the degeneracy, and  $m^*$  the excitonic mass.

The legitimacy of this analysis has been questioned in Ref. 14, where it was argued that Auger processes might lead to a serious overestimation of the exciton density. Subsequent experimental studies,<sup>15</sup> however, have shown that this is only relevant near the surface. The experiments described here use excitation in the near infrared, where the optical penetration depth is larger than  $500 \mu\text{m}$ .<sup>16</sup> Any contribution due to surface enhanced Auger processes is therefore expected to be negligible. For the same reason (large penetration depth) the thus created exciton gas is nearly uniformly distributed in the sample. Therefore effects related to a strong spatial inhomogeneity of the gas can also be neglected in our case.

## II. PHOTOLUMINESCENCE EXCITATION SPECTROSCOPY

The samples used in this study were [100] platelets cut from a single crystal grown by a floating zone technique.<sup>17</sup> The upper limit for the full width at half maximum of the ortho-exciton direct emission at  $T=10\text{K}$  is measured to be  $0.09\text{meV}$  ( $0.3\text{meV}$ ) which is an experimental resolution limited result. The excitonic emission is observed up to the room temperature. In the emission spectrum obtained for overbandgap excitation ( $E > 2.17$  eV) a broad band is observed peaked at  $1.7$  eV attributed to ionized oxygen vacancy  $V_{\text{O}}^{2+}$ .<sup>18</sup> The relative intensity of the ( $X_{\text{ortho}}$ ) and  $V_{\text{O}}^{2+}$  bands is comparable to those reported for high quality samples and shows that the samples used in this study have a relatively low density of the oxygen vacancies. Emission peaks attributed to excitons bound to impurities that have been reported around  $2\text{eV}$  are absent in our spectra.<sup>18</sup> Moreover we observe an exceptionally long lifetime of paraexcitons in our samples,  $\tau \approx 14$  ms,<sup>19</sup> independently demonstrating the high quality of the sample since the decay of paraexcitons is exclusively defect limited.

For the photoluminescence excitation experiments samples were polished and mounted on the cold finger of a continuous flow cryostat and kept at  $T = 4$  K. The time integrated experiments were performed using an optical parametric amplifier pumped by the third harmonic of a 10 Hz Nd:YAG laser. Excitation pulses with photon energies in the  $1 - 2.5$  eV range and temporal width of 8 ns were weakly focused on the sample (spot size  $500 \mu\text{m}$ ). The yellow exciton emission was detected in a back-reflection geometry using a 0.5 m double-grating monochromator in combination with a photomultiplier.

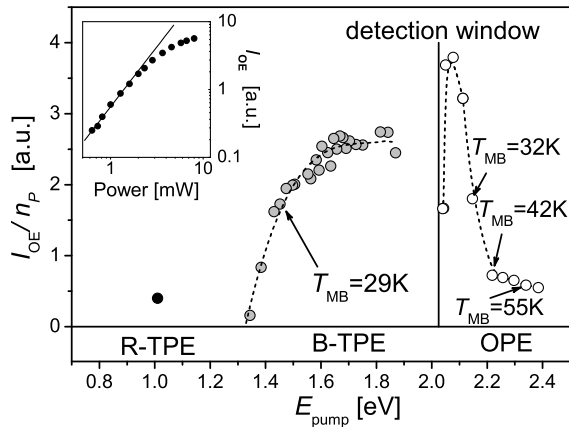


FIG. 2: Integrated intensity of the ortho-exciton emission per incoming photon ( $I_{OE}/n_p$ ) versus the pump laser energy ( $E_{\text{pump}}$ ). Bath temperature  $T = 7$  K,  $P = 3$  mW = constant. Full circles - Blue-exciton Two Photon Excitation (B-TPE), open circles - One Photon Excitation (OPE) and black dot - 1s Resonant Two-Photon Excitation (R-TPE). Dashed lines are guides to the eye. Inset:  $I_{OE}$  as a function of the pumping laser power for  $E_{\text{pump}} = 1.4$  eV. Solid line shows a fit for  $I \sim P^\alpha$  with  $\alpha = 1.8$ .

Figure 2 shows the results of a photoluminescence excitation study of yellow exciton creation in  $\text{Cu}_2\text{O}$ . During the experiments the pump fluency was kept constant at  $30 \text{ W/cm}^2$ . The integrated intensity  $I_{OE}$  of the ortho-exciton emission (both phonon-assisted and direct) is normalized by the number of incoming photons per second  $n_p$ , and is therefore a measure of the efficiency of the pumping.

Optical pumping is the most commonly used method to produce excitons. The efficiency of creating the excitonic gas will naturally depend on the particular process involved, and hence on the pump photon energy  $E_{\text{pump}}$ . The observed excitation spectrum may be divided into several regions representing different excitation processes. A first rough division can be made into a one-photon (OPE) and a two-photon (TPE) excitation region, with the divider at the 1s exciton energy. In the high energy OPE region ( $E_{\text{pump}} > E_{\text{gap}} \approx 2.17$  eV) the dominant process is direct excitation of electron-hole ( $C_1 - V_1$ ) pairs, which may subsequently form an exciton. As mentioned above, however, this process is not very effective due to the even parity of both bands involved. For  $E_{\text{pump}} < E_{\text{gap}}$  the process becomes more efficient since single photon transitions to excited yellow exciton states as well as resonant Raman transitions are allowed. The OPE efficiency reaches its maximum when  $E_{\text{pump}}$  approaches  $X_{\text{ortho}}^{\text{DI}} + \text{LO}$  at  $2.05$  eV<sup>20</sup> and decreases gradually upon increasing excitation energy. It agrees with the fact that the absorption coefficient at the excitonic states of higher quantum number  $n$  decreases as  $\approx 1/n^3$ . Decrease of the number of free excitons created by pumping photon may also be related to the fact that overbandgap excitation enables retrapping of either electrons or hot-excitons by defect sites.<sup>21</sup> Moreover a surface photo-voltage effect may take place, which leads to a space-charge accumulation at the surface.

Resonant two photon excitation (R-TPE, black data point at  $1.015$  eV) to the ortho-exciton state is allowed by symmetry and could thus, in principle, be efficient. Unfortunately, the matrix element for this process is fairly small since it involves an intermediate state which lies as deep as  $5.6$  eV below the upper valence band ( $V_1$ ),<sup>22</sup> in agreement with the low efficiency observed.

The so far unexplored part of the excitation spectrum is the  $1.3$ - $1.9$  eV region. Surprisingly efficient excitation of the  $2.036$  eV yellow ortho-excitons is observed for  $E_{\text{pump}}$  significantly below  $X_{\text{ortho}}$  but still well above  $X_{\text{ortho}}/2$ . The precise nature of the process responsible will be discussed later on. At this point, it is sufficient to note that it is a two photon process with  $V_1 - C_2$  electron-hole pairs as intermediate state. This is evidenced by the observation of a threshold for the process at  $\sim 1.3$  eV which coincides with half the  $V_1 - C_2$  energy gap and by the near quadratic dependence of the excitonic emission on the fluency (see inset Fig. 2) measured for  $E_{\text{pump}} = 1.4$  eV.

The origin of the saturation of the efficiency for high fluencies ( $P \gg 40 \text{ W/cm}^2$ ) remains to be investigated. It has also been observed for other excitation methods, and may originate from two-exciton spin-flip processes.<sup>23</sup>

For the quest for Bose-Einstein condensation in excitonic matter it is vital to have an efficient excitation process (*i.e.* a high density). The limited lifetime of the exciton gas, however, also imposes the requirement of a low initial exciton gas temperature. At first sight, this seems problematic for the new B-TPE process. The process has an excess energy of at least  $0.5$  eV, which might be dissipated in either the exciton gas or in the lattice. A first estimate of the temperature of the gas can be made by fitting Eq.(1) to the PA band (see Fig. 1), using the Maxwell-Boltzmann distribution. The thus obtained gas temperatures are denoted in Fig. 2 for several OPE and B-TPE excitation energies. In all cases the exciton temperature is higher than the bath temperature ( $4$  K). In the OPE region, the smaller the energy mismatch between  $E_{\text{pump}}$  and  $X_{\text{ortho}}$ , the lower  $T_{\text{mb}}$ . It decreases from  $55$  K for  $E_{\text{pump}} = 2.3$  eV

to 32 K for 2.15 eV. Surprisingly, an even lower gas temperature is observed when  $1.4 < E_{\text{pump}} < 1.9$  eV in spite of the fact that the energy mismatch (0.1-0.7 eV) is much larger than in the OPE cases. The exciton temperature in this range is found to be 29 K, nearly independent on the photon energy. Apparently, the excess energy leaves the system. One possibility would be that the  $V_1 - C_2$  electron-hole state decays to the yellow exciton state through a dipole allowed transition either direct, or via an intermediate  $V_1 - C_1$  electron-hole state. Another possibility is that the  $V_1 - C_2$  state acts as an intermediate state for a hyper-Raman type process. In both cases the excess energy is emitted as a photon, which, in view of the low absorption coefficient at low energy, would indeed leave the sample. For determination of the precise nature of the process involved, one would need to perform emission experiments in the energy range 0.1-0.7 eV.

### III. TIME RESOLVED TWO PHOTON SPECTROSCOPY

A more detailed insight into the properties of the B-TPE created exciton gas may be obtained from time-resolved luminescence experiments. Time resolved measurements were performed using a traveling wave optical parametric amplifier pumped by 1 kHz, 1.55 eV, 120 fs pulses produced by an amplified Ti-Sapphire laser system. The 150 fs excitation pulses (1.3-2.5 eV) were focused on the sample with a spot size of about  $100\mu\text{m}$ . The exciton emission was detected by a Hamamatsu streak camera system operating in photon counting mode (temporal resolution 10 ps). The experimental spectral resolution function is measured to be of a Gaussian type with  $\Gamma=0.37\text{nm}$ .

Figure 3 shows the time-resolved ortho-exciton luminescence spectra after excitation with a 150 fs pulse ( $E_{\text{pump}}=1.4$  eV) at  $T = 7$  K. Initially, a broad spectrum is observed dominated by the phonon assisted transitions reflecting the relatively high excitonic temperature. Despite the rather indirect way of excitation, no initial growth of the luminescence has been observed, and the exciton creation appears to be instantaneous upon excitation within the experimental resolution (10 ps). As time progresses both the intensity and the shape of the emission change, where the former reflects the cooling of the exciton gas, and the latter the temporal decay of the exciton population. Direct and phonon-assisted peaks become well resolved for delay times longer than 0.2 ns, and show a similar long time decay dynamics.

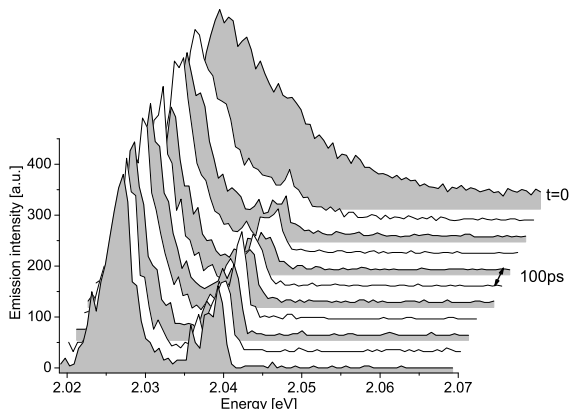


FIG. 3: Time evolution of the ortho-exciton emission spectrum after excitation with a 150 fs,  $E_{\text{pump}}=1.4$  eV pulse.

Two representative time-resolved  $X_{\text{ortho}}$  luminescence spectra are shown in figure 4, recorded 250 and 950 ps after excitation with a 150 fs pulse with  $E_{\text{pump}}=1.4$  eV, together with fits to Eq.(1), using a Bose-Einstein distribution function. The values for the gas temperatures at these times are found to be  $T = 34$  K, and  $T = 17$  K, respectively. As one can see, the fits reproduce the high energy tail very well. The deviations observed at the onset of the emission are due to replica-like structures which presumably appear due to a small strain induced by the mounting of the sample on the cold finger of the cryostat.<sup>24</sup> In the final fitting of the data this was taken into account by adding a scaled down replica of the spectrum, shifted by about 3 meV to Eq.(1).

The parameters resulting from fitting Eq.(1) to time resolved spectra of the phonon assisted luminescence are shown in Fig. 5 (upper panels). The two parameter sets shown correspond to experiments with excitation with 1.4 eV (filled symbols) and 2.17 eV (open circles), *i.e.* to B-TPE and OPE excitation, respectively. The cooling of the gas, shown in Fig. 5a), shows a bi-exponential behavior. Initial fast cooling ( $\tau \sim 0.2$  ns) occurs via optical phonon emission. Once the kinetic energy of the excitons becomes too low for this process, the relaxation occurs via acoustical phonon emission with a relatively long decay time ( $\tau \sim 6$  ns). Though the cooling rate hardly depends on the excitation method, it is clear from the figure that B-TPE excitation yields lower gas temperatures due to the lower initial

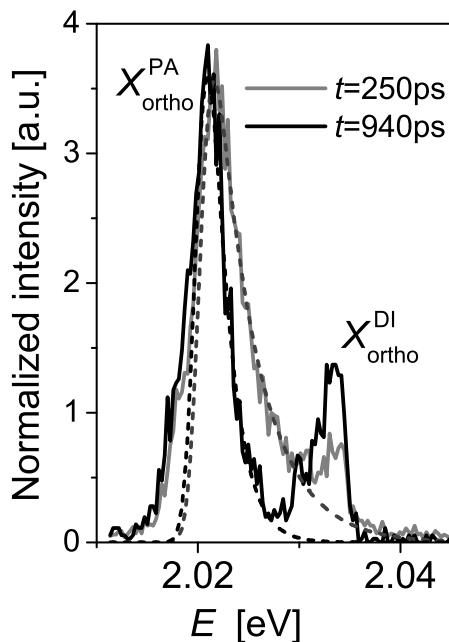


FIG. 4: Left panel: Schematic energy band diagram at the  $\Gamma$  point in  $\text{Cu}_2\text{O}$ . Right panel: Time resolved ortho-exciton emission spectra at  $t = 250$  ps and  $t = 940$  ps. Dashed lines are a fit to Eq.(1) using Bose-Einstein statistics with  $T_{\text{be}} = 64$  K;  $\mu = -0.7$  meV, and  $T_{\text{be}} = 23$  K;  $\mu = -0.24$  meV, respectively.

temperature. The chemical potential, shown in Fig. 5b), decays faster than the temperature, with a time constant  $t \sim 1.2$  ns. This decay is essentially due to loss of particles. Consistently, the integrated intensity (Fig. 5c) of the luminescence shows a similar decay time ( $t \sim 1.4$  ns). The conversion of ortho-excitons into para-excitons, the main cause of the loss of particles, strongly depends on temperature, hence the non-exponential behavior at early times.<sup>15</sup> The observation that the particle decay is faster than the cooling rate, makes it implausible that the gas would undergo a BEC transition. This is demonstrated in the inset of Fig. 5a), which shows the  $(n, T)$  phase diagram. The state of the gas follows the BEC phase boundary, and no crossing is observed, similar to earlier observations.<sup>12</sup> Apparently, the gas adjusts its quantum properties to the density and temperature and is in quasi-equilibrium.

As the gas cools down the relative occupation of the  $k \approx 0$  state is expected to increase. Indeed, the direct emission initially increases (see Fig. 5c), and the ratio of direct to phonon assisted emission increases with time (decreases with temperature, Fig. 5d). For B-TPE excitation this ratio is higher than for OPE excitation for given  $T_{\text{BE}}$ . One can therefore conclude that the B-TPE process leads to a preferential occupation of the  $k \approx 0$  state, which in itself is favorable for BEC condensation.

Different explanations have been proposed for the so-called “quantum saturation” effect. In Ref. 25 it has been suggested that the quantum saturation phenomenon originates from the fact that the ortho-gas is not in an equilibrium state so that the number of ortho-excitons is not well defined. As a consequence  $\mu = 0$  by definition and no phase transition is possible. The present results do not support this conclusion. The kinetic energy distribution of the ortho-gas can be described with a very good accuracy by the BE distribution, and moreover decay of the chemical potential coincides with the particle decay obtained independently from the emission intensity decay. Therefore, one may conclude that the ortho-gas is in fact in quasi-equilibrium, and the particle density is a well defined number. Apparently the exciton gas adjusts its properties even though the phase boundary is not crossed. Kavoulakis<sup>23</sup> has argued that the above mentioned fitting based analysis to extract the exciton temperature and density is misleading since the ortho-gas is not in a quantum state but in a normal state and under this assumption the gas slides along adiabats given by  $n/n_Q \sim 0.01$ , where  $n_Q$  is the quantum concentration. However, for this to be true, it would require an overestimation of the exciton density by two orders of magnitude, and it does not explain how a classical gas can show a non-classical kinetic-energy distribution. A few possible explanations for an apparent non-classical distribution have, however, been given in literature: dominant Auger recombination and/or strong spatial inhomogeneity. As has been discussed in section I, both effects are expected to have only a marginal influence on the decay kinetics for B-TPE excitation. Since for OPE pumping similar results are found, the significance of these two effects is questionable in that case as well. Finally, Ell *et al.*<sup>26</sup> presented an analysis of the ortho-exciton relaxation which included polaritonic effects. The main conclusion of that analysis is that the so called polaritonic “bottleneck effect” prevents formation

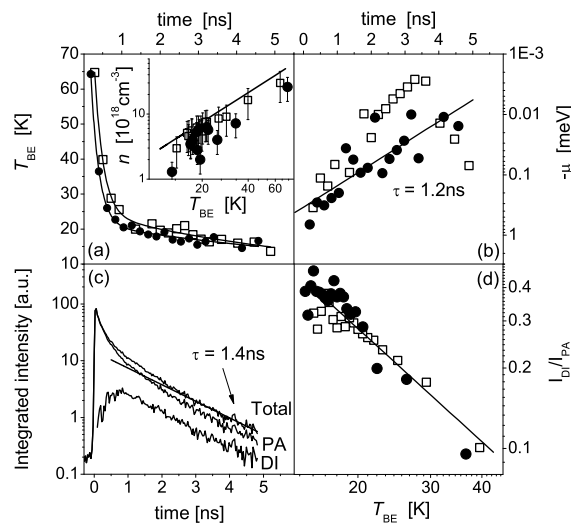


FIG. 5: Upper panels: Time dependence of (a) the exciton temperature  $T_{\text{be}}$  and (b) chemical potential. Solid lines are fits to a two- and one-exponential decay, respectively. The inset in (a) shows the  $n, T$  phase diagram (solid line is the BEC boundary), where  $n$  has been calculated using Eq.(2).

Lower panels: (c) Temporal decay of the integrated intensities of the total, direct (DI), and phonon assisted (PA) luminescence. Solid line: fit to a single exponential decay. (d) Ratio between direct and phonon assisted luminescence as function of the gas temperature, solid lines are a guide to the eye. The data sets are for  $E_{\text{pump}}=1.4$  eV (circles), and  $E_{\text{pump}}=2.17$  eV (squares).

of an ortho-excitonic BEC at  $k=0$ . However, as pointed out in Ref. 27, the authors assumed in their model an infinite volume and it is not clear to what extent their conclusions would change due to finite volume corrections. From the above analysis we can conclude that only the third model does not contradict with the present results but the full model is still to be established.

Aware of the limitations mentioned in the introduction, we applied the same analysis to  $E_{\text{pump}}=2.17$  eV data, where the penetration depth is only  $30 \mu\text{m}$ , and the results lead to similar conclusions as in the B-TPE case. The fact that the early time density reached for  $E_{\text{pump}}=2.17$  eV excitation is significantly higher than for  $E_{\text{pump}}=1.4$  eV excitation agrees well with the  $\sim 10$  times smaller penetration depth, and the 5 times lower pumping efficiency. This indirectly supports the use of Eq.(2), even in the case of a small penetration depth.

#### IV. POLARITON OSCILLATIONS

Analysis of the  $X_{\text{ortho}}$  emission presented in the previous sections shows that absorption of the pump photons results in the formation of ortho-exciton through a fast and efficient process. The intensities of both  $X_{\text{ortho}}^{\text{PA}}$  and  $X_{\text{ortho}}^{\text{DI}}$  emission decay mainly as a result of down-conversion of the ortho-excitons into para-excitons. More detailed analysis of the  $X_{\text{ortho}}^{\text{DI}}$  however reveals also weak oscillations in the measured  $X_{\text{ortho}}^{\text{DI}}$  emission intensity ( $I_{\text{od}}$ ), reminiscent of those previously observed by Fröhlich et al.<sup>10,11</sup> This is shown in Fig. 6, which displays the time dependence of the intensity after subtraction of a smooth exponential decay curve. The oscillations have a typical “period” of about 0.5 ns, which increases with time as  $\sqrt{t}$  (see also inset fig.6). They are thought to originate from interference between states of the lower and upper polaritonic branches.<sup>10,11</sup> Such oscillations have so far only been observed for resonant one-photon excitation in a transmission geometry, and it is not immediately clear that the polaritonic interference would be relevant to the present two-photon experiment and a B-TPE excitation scheme. In the following section we therefore make an excursion to the semiclassical theory of the polariton oscillations of transmitted light, which allows us to obtain an analytical expression for these oscillations. Most importantly, the results obtained in Sec. V can be generalized to describe more complicated processes, such as the present time resolved two photon experiment. This is done in Sec. VI, where we show that the aperiodic oscillations presented in Fig. 6 indeed result from the polariton beating.

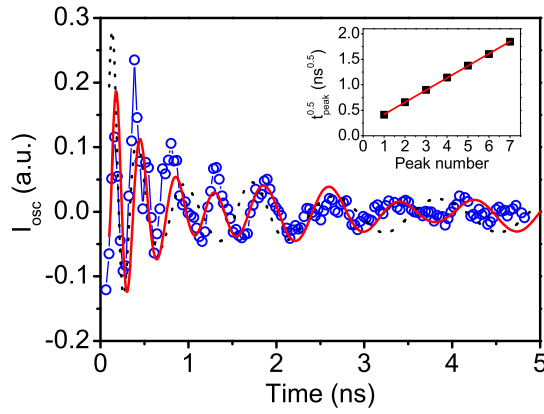


FIG. 6: Direct emission versus time from figure 5(c) after subtraction of a single exponential decay curve (symbols). Dashed and solid lines: theoretical simulation as discussed in section VI. The inset shows the  $\sqrt{t}$  dependence of the peak positions.

## V. POLARITON OSCILLATIONS IN TRANSMISSION OF LIGHT AND GEOMETRICAL OPTICS

In this section we give a semiclassical description of the polariton oscillations, observed in the transmission experiment on  $\text{Cu}_2\text{O}$ .<sup>10,11</sup> In principle, the transmission intensity can be found by a straightforward numerical calculation, as was done in Ref.[10]. Here we obtain an accurate analytical expression for this intensity.

Consider the propagation of linearly polarized light with frequency  $\omega$  through a slab of a material with dielectric function  $\epsilon$  (see Fig. 7). For a monochromatic incident electric field  $E_i = E_0 e^{-i\omega t + ikx}$ , where  $k = \frac{\omega}{c}$ , the amplitude of the transmitted field is

$$E_t = E_0 e^{-i\omega t + iqL} \frac{(1 - R^2)}{1 - R^2 e^{2iqL}}, \quad (3)$$

where  $L$  is the slab thickness,  $q = \frac{\omega}{c} \sqrt{\epsilon}$ , and  $R = \frac{\sqrt{\epsilon} - 1}{\sqrt{\epsilon} + 1}$  is the reflection amplitude. Equation (3) allows for a simple interpretation: the electric field is multiplied by the factor  $1 - R$  when the light enters the material, and by  $1 + R$  when it gets out,  $-i\omega t + iqL$  is the phase acquired by the light traveling through the sample during the time  $t$ , and the denominator

$$\frac{1}{1 - R^2 e^{2iqL}} = 1 + R^2 e^{2iqL} + R^4 e^{4iqL} + \dots,$$

is the sum over the number of internal reflections from the boundaries the slab (see Fig. 8): a factor  $R$  for each internal reflection and  $e^{iqL}$  for the propagation from one side of the slab to the other side.

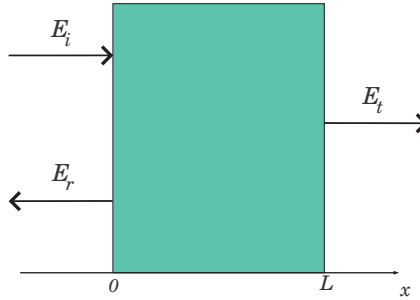


FIG. 7: The transmission of light propagating in the  $x$  direction through the slab.

Consider now the incident electric field having the form of the Gaussian wave packet with the average frequency  $\bar{\omega}$  and width  $\Delta$ :

$$E_{in} = \frac{E_0}{\sqrt{2\pi}\Delta} \int d\omega e^{-i\omega t + ikx - \frac{(\omega - \bar{\omega})^2}{2\Delta^2}}.$$

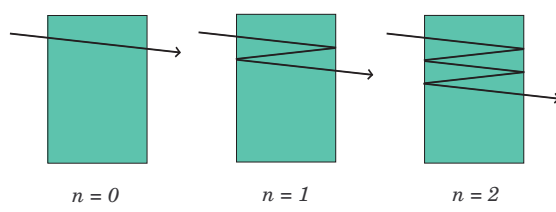


FIG. 8: Examples of processes with different numbers of internal reflections.

Then the transmitted field at  $x = L$  is given by

$$E_t = \frac{E_0}{\sqrt{2\pi}\Delta} \sum_{n=0} \int d\omega (1 - R^2) R^{2n} e^{iS_n - \frac{(\omega - \bar{\omega})^2}{2\Delta^2}}, \quad (4)$$

where the action  $S_n = -\omega t + q(2n + 1)L$  is the phase of the field for a path with  $2n$  internal reflections. Since  $L$  is usually much larger than the wavelength, the integral in Eq.(4) can be calculated in the stationary phase approximation:

$$E_t \approx E_0 \sum_{n=0} \frac{(1 - R^2) R^{2n}}{\sqrt{1 - i(2n + 1)L\Delta^2 \frac{d^2q}{d\omega^2}}} e^{iS_n - \frac{(\omega_n - \bar{\omega})^2}{2\Delta^2}}, \quad (5)$$

where the values of  $S_n$ ,  $\frac{d^2q}{d\omega^2}$ , and  $R$  are taken at the ‘stationary’ frequency  $\omega_n$ , such that

$$\frac{dS_n}{d\omega}(\omega_n) + i \frac{(\omega_n - \bar{\omega})}{\Delta^2} = -t + \frac{dq}{d\omega}(2n + 1)L + i \frac{(\omega_n - \bar{\omega})}{\Delta^2} = 0. \quad (6)$$

For a broad wave packet, the term  $\propto \frac{1}{\Delta^2}$  can be neglected and we obtain

$$\left. \frac{d\omega}{dq} \right|_{\omega=\omega_n} = \frac{(2n + 1)L}{t}, \quad (7)$$

which is the geometrical optics result: the group velocity of light in the slab equals the path  $(2n + 1)L$  divided by the time of motion  $t$ . Furthermore, for a broad wave packet

$$E_t \approx E_0 \sum_{n=0} \frac{\Delta_n}{\Delta} (1 - R^2) R^{2n} e^{i(S_n + \frac{\pi}{4})}, \quad (8)$$

where  $\Delta_n = \left[ (2n + 1)L \frac{d^2q}{d\omega^2} \right]^{-1/2} \ll \Delta$  is the width of the frequency interval around  $\omega_n$  that gives the dominant contribution to the integral in Eq.(4).

If there are no excitations with  $\omega \sim \bar{\omega}$  present in the sample,  $\epsilon$  is a slow function of frequency and can be replaced by a constant  $\epsilon_0 = \epsilon'_0 + i\epsilon''_0$ . The time it takes light to traverse the sample is then  $t_0 = \frac{L}{c} \sqrt{\epsilon'_0}$  (for a 1mm slab of  $\text{Cu}_2\text{O}$  with  $\epsilon'_0 = 6.5$ ,  $t_0 = 8.5\text{ps}$ ). If the time  $t$  between the moment the light enters the sample and the moment it is observed on the other side of the sample greatly exceeds  $t_0$ , then one way to satisfy Eq.(7) would be to consider processes, in which the light is reflected many times ( $n \gg 1$ ) and passes a long way  $(2n + 1)L$  before it leaves the sample. Due to the rather strong absorption of visible light in  $\text{Cu}_2\text{O}$  and the loss of intensity at each reflection (the reflection coefficient  $R^2 \approx 0.2$ ), the intensity of the transmitted light for  $n \gg 1$  is extremely weak.

Equation (7) can also be satisfied for small  $n$ , but only if light in the sample can propagate slowly. This happens when it is mixed with an exciton, i.e. when  $\bar{\omega} \approx \Omega$ , where  $\Omega$  is the exciton frequency. Such a mixing results in two polariton branches  $\omega_{\pm}(q)$ , both containing slowly propagating excitations (see Fig. 9), so that Eq.(7) has two solutions. Then Eq.(8) has to be modified and for each  $n$  the transmitted field is the sum of the contributions of the two polariton trajectories:

$$E_t \approx 2E_0 \sum_{n=0} \frac{\Delta_n}{\Delta} (1 - R^2) R^{2n} e^{i \frac{(S_{n+} + S_{n-})}{2}} \cos \left( \frac{S_{n+} - S_{n-}}{2} + \frac{\pi}{4} \right), \quad (9)$$

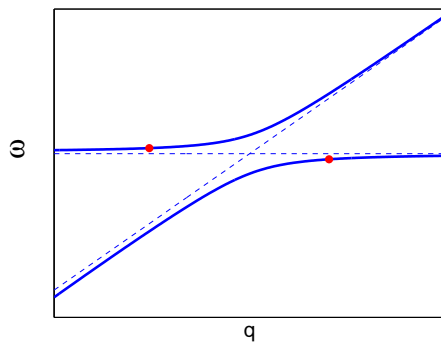


FIG. 9: Two branches of the polariton dispersion (solid lines). The circles mark a pair of polaritons moving with the same velocity.

where  $\pm$  labels the polariton branch. Below we show that for the quadrupolar of excitons to light  $\frac{S_{n+}-S_{n-}}{2} = \Omega\sqrt{(2n+1)ftt_0}$ , where  $f$  is the strength of the quadrupolar coupling, so that the interference between the two polaritons moving with the same velocity gives rise to oscillations of the intensity of the transmitted light with a time-dependent period. Equation (9) is actually an asymptotic expression for  $E_t$  valid in the large- $t$  limit, when  $\omega_{n+} - \omega_{n-} \gg \Delta_n$ , i.e. when the intervals of relevant frequencies around the two stationary points do not overlap. A more general expression is obtained below [see Eq.(16)]. A similar situation is found in scattering problems, when the interference between different classical trajectories makes the scattering cross-section a rapidly oscillating function of angle. A simple semiclassical expression for the cross-section is not valid, however, for angles close to 0 and  $\pi$ , where the so-called glory phenomenon takes place.<sup>28</sup>

The polariton dispersion is found from

$$(\omega^2 + i\omega\Gamma - \varepsilon_q^2)(\omega^2 - \omega_q^2) - f\omega^2\omega_q^2 = 0, \quad (10)$$

where  $\omega_q = \frac{cq}{\sqrt{\varepsilon_0}}$  and  $\varepsilon_q = \Omega + \frac{q^2}{2M}$  are, respectively, the photon and exciton frequencies,  $f$  is the strength of the quadrupolar photon-exciton coupling and  $\Gamma$  is the exciton decay width. Equation (10) corresponds to the dielectric function<sup>10,11</sup>

$$\epsilon(\omega, q) = \epsilon_0 + \frac{fc^2q^2}{\varepsilon_q^2 - \omega^2 - i\omega\Gamma}. \quad (11)$$

It is convenient to introduce the dimensionless variables  $X = \frac{c^2q^2}{\Omega^2\varepsilon_0}$  (wave vector squared) and  $Y = \frac{\omega^2}{\Omega^2}$  (frequency squared), which near the crossing point of the photon and exciton dispersions are both close to 1. We also make use of the fact that for Cu<sub>2</sub>O the dimensionless parameters, describing the exciton-photon coupling ( $f \approx 4 \cdot 10^{-9}$ ), exciton kinetic energy ( $\xi = \epsilon_0' \frac{\Omega}{Mc^2} \approx 10^{-5}$ ), decay width ( $\gamma = \frac{\Gamma}{\Omega} \approx 5 \cdot 10^{-7}$ ),<sup>10,11</sup> and the absorption of light ( $\zeta = \frac{\epsilon_0''}{\epsilon_0} \approx 10^{-4}$ ) are rather small. Then Eq.(10) can be written in the form

$$(Y - 1 - \xi + i\gamma)(Y - X + i\zeta) = f. \quad (12)$$

Near the photon-exciton crossing point

$$\begin{cases} X = 1 + \xi + X', \\ Y = 1 + \xi + Y', \end{cases}$$

with  $X', Y' \ll 1$ . Using Eq.(12) we can express the polariton ‘momentum’  $X'$  in terms of its ‘frequency’  $Y'$ :

$$X' = Y' - \frac{f}{Y' + i\gamma} + i\zeta. \quad (13)$$

Note that while  $X'(Y')$  is a single-valued function,  $Y'(X')$  has two branches.

The polariton action is then given by

$$S_n = -\omega t + q(2n+1)L \approx \Omega[(2n+1)t_0 - t] + \frac{\Omega t}{2}[r_n X' - Y' - \xi], \quad (14)$$

where  $r_n = (2n+1)\frac{t_0}{t}$  and, by assumption,  $r_n \ll 1$ . Using the substitution  $Y' = z\sqrt{fr_n}$  and Eq.(13), we obtain

$$S_n \approx S_n^{(0)} - \frac{\phi_n}{2} \left[ z + \frac{1}{z + i\frac{\gamma}{\sqrt{fr_n}}} \right]. \quad (15)$$

Here  $S_n^{(0)} = \Omega[(2n+1)t_0 - t] + i\Omega(2n+1)t_0\frac{\zeta}{2}$  is the action for  $f = 0$  and  $\phi_n = \Omega t\sqrt{fr_n} = \Omega\sqrt{(2n+1)ftt_0}$  is the phase of the polariton oscillations. Equation (4) can now be written in the form

$$E_t \approx E_0 (1 - R^2) \sum_{n=0} \frac{\Delta_n}{\Delta} R^{2n} e^{iS_n^{(0)}} I\left(\phi_n, \frac{\gamma}{\sqrt{fr_n}}, \frac{\phi_n}{2\Delta t}, \frac{\xi}{\sqrt{fr_n}}\right), \quad (16)$$

where  $\Delta_n^2 = \frac{\Omega\sqrt{fr_n}}{4t}$ ,  $R = \frac{\sqrt{\epsilon_0' - 1}}{\sqrt{\epsilon_0' + 1}}$ , and

$$I(a, b, c, d) = \sqrt{\frac{a}{2\pi}} \int_{-\infty}^{+\infty} dz e^{-i\frac{a}{2}\left(z + \frac{1}{z+ib}\right) - \frac{c}{2}(z+d)^2} \quad (17)$$

The factor  $e^{-\frac{c}{2}(z+d)^2}$  (with  $c = \left(\frac{\alpha_n}{2\Delta t}\right)^2$  and  $d = \frac{\xi}{\sqrt{fr_n}}$ ), describing the shape of the Gaussian wave packet with  $\bar{\omega} = \Omega$ , is only important for  $a \lesssim 1$ . For  $a \gg 1$ ,  $I(a, b, c, d)$  becomes independent of  $c$  and  $d$ . In this limit the integration over  $z$  can be done in the stationary-phase approximation, as the two stationary points  $z_{n\pm}$ :  $z_{n\pm} + i\beta_n = \pm 1$ , are sufficiently separated from each other. The result is

$$I(a, b, c, d) \approx 2e^{-\frac{ab}{2}} \cos\left(a + \frac{\pi}{4}\right). \quad (18)$$

In Fig. 10 we compare  $I(a, b, c, d)$ , defined by Eq.(17), for  $b = c = 0.1$  and  $d = 0$  (dots), with the asymptotic expression Eq.(18) (solid line). We see that after about one oscillation the two curves coincide and the transmitted field equals the sum of the two polariton contributions

$$E_t \approx 2E_0 (1 - R^2) \sum_{n=0} R^{2n} e^{i\Omega[(2n+1)t_0 - t] - \frac{1}{2}\alpha_\Omega(2n+1)L - \frac{\Gamma t}{2}} \frac{\Delta_n}{\Delta} \cos\left(\Omega\sqrt{(2n+1)ftt_0} + \frac{\pi}{4}\right) \quad (19)$$

[cf. Eq.(9)], where  $\alpha(\Omega) = \frac{\Omega\epsilon_0''}{c\sqrt{\epsilon_0'}}$  is the absorption coefficient at the frequency  $\Omega$ .

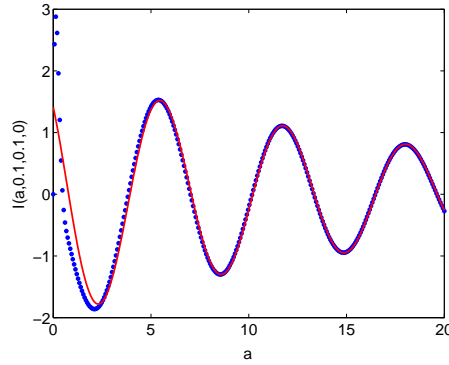


FIG. 10: The  $a$ -dependence of the integral  $I(a, 0.1, 0.1, 0)$  [see Eq.(17)] calculated numerically (dots) and in the stationary phase approximation (solid line).

For further discussion it is useful to note that Eq.(19) can be written in the form

$$E_t \approx E_0 (1 - R^2) \sum_{n=0} R^{2n} F(l_n, t), \quad (20)$$

where  $F(l, t)$  is a function of the length of the polariton path  $l$  and the time of motion  $t$ :

$$F(l, t) = 2e^{i\Omega \left[ \frac{l\sqrt{\epsilon_0'}}{c} - t \right] - \frac{1}{2}\alpha(\Omega)l - \frac{\Gamma t}{2}} \frac{\Delta(l)}{\Delta} \cos \left( \Omega \sqrt{\frac{ftl\sqrt{\epsilon_0'}}{c}} + \frac{\pi}{4} \right), \quad (21)$$

$$l_n = (2n + 1)L \text{ and } \Delta(l) = \Delta_0 \left[ \frac{l}{L} \right]^{\frac{1}{4}}.$$

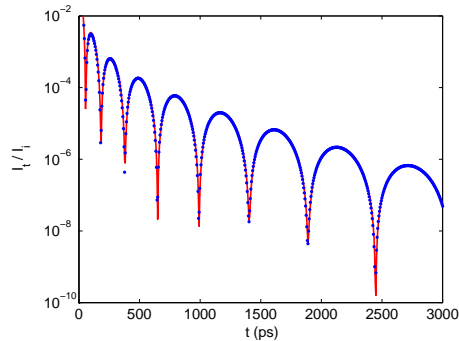


FIG. 11: The ratio of the intensities of the transmitted and incident light for the parameters taken from Ref. [10,11] calculated numerically using Eq.(16) (dots) and in the stationary phase approximation (solid line).

The ratio of the intensities of the transmitted and incident light for the parameters taken from Ref. [10,11] is shown in Fig. 11. The results of the numerical calculation of Eqs.(16) and (17)] are plotted with dots, while the solid line was obtained using the semiclassical expression Eq.(19). The difference between the two is hardly visible in this semi-logarithmic plot, even for short times  $\sim 30$  ps. For the rather thick sample used in that experiment ( $L = 0.91\text{mm}$ ) the contributions of the processes with multiple internal reflections are negligibly small:  $\frac{I_t(n=1)}{I_t(n=0)} \approx 2 \cdot 10^{-3}$ , so that the transmitted intensity shows a single-mode oscillation, the period of which grows with time.

## VI. POLARITON OSCILLATIONS IN NON-LINEAR PROCESS

In this section we return to the present experiments and apply the semiclassical formalism discussed in the previous section to a non-linear process, in which two photons with the frequency  $\omega_0$  are converted into a photon with the frequency close to the ortho-exciton frequency  $\Omega < 2\omega_0$ . Our aim is to explain the oscillations of the emitted light shown Fig.6. Although small in amplitude and somewhat irregular, these oscillations occur on the same time scale (of a few hundred picoseconds) as the oscillations of the transmitted light, discussed in Sec.V. Furthermore, the inset in Fig.6 shows the phase of these oscillations grows proportionally to square root of time, just as in the transmission experiment. Clearly, the intensity oscillations observed in our experiment result from the polariton beating.

This conclusion is actually very surprising, since the polariton effects seem to be incompatible with the high-density exciton gas, achieved in the present set-up. The exciton collision time in a gas with the density  $n = 10^{19}\text{cm}^{-3}$  and temperature  $T = 30\text{K}$  is  $\tau \sim 0.06\text{ps}$ , which is three orders of magnitude smaller than the oscillation period  $\sim 500\text{ps}$ . Furthermore, the polariton momentum  $p_p = \sqrt{\epsilon_0} \frac{\Omega}{c}$  is much smaller than the width of the thermal distribution in the exciton gas  $p_T = \sqrt{3MT}$ :  $p_p \sim 0.1p_T$ . Thus the elastic collisions effectively suppress the polariton oscillations by removing very fast the excitons from the momentum range, in which their interaction with light is important. The intensity oscillations may only come from polaritons propagating through the regions where the exciton gas density is sufficiently low. In our experimental set-up the incoming light falls at a small angle  $\sim 10^\circ$  with respect to the surface normal, while the aperture angle was made rather large  $\sim 20^\circ$  to increase the signal-to-noise ratio. This allows polaritons, created at the rims of the light spot, to reach detector without passing through the dense exciton gas regions. The fact that the exciton cloud grows with time does not alter this conclusion. While the polariton momentum is much smaller than the thermal momentum, the polariton velocity  $v_p \sim \frac{c}{\sqrt{\epsilon_0}} \frac{t_0}{t}$ , where  $t \sim 2\text{ns}$  is the time of the polariton motion, is much larger than the thermal velocity  $v_T = \sqrt{\frac{3T}{M}}$ :  $v_p \sim 20v_T$ . Furthermore, the length of the polariton path  $\sim L$  covered during that time is much larger than increase of the size of the exciton cloud  $\sim \sqrt{6v_T^2 t \tau}$ , so that polaritons can escape the expanding exciton cloud.

The essential difference between the non-linear and transmission experiments is the energy and momentum dissipation, which occurs when the two in-coming photons are converted into a slowly propagating polariton. As details

of this process are poorly understood, we simply assume here that the conversion is fast (on the scale of the polariton oscillations) and that it occurs locally, i.e. the polaritons are almost immediately emitted from the spot, where the two photons were absorbed. Furthermore, we assume that after the short thermalization time the motion of slow polaritons (with the frequency close to  $\Omega$ ) is essentially free, i.e. their interactions with phonons and other excitons can be neglected. In the transmission experiment<sup>10,11</sup> the frequency of the incident light was deliberately chosen to be close to the exciton frequency  $\Omega$  to maximize the amplitude of the polariton oscillations. In the nonlinear experiment one obtains an exciton gas with a broad thermal distribution. The energy and momentum selection of the excitons occurs in this case automatically, since only the excitons with the energy close to  $\hbar\Omega$  are strongly mixed with light and contribute to the polariton oscillations, and only those moving in the directions approximately parallel and antiparallel to the sample surface normal have a chance to be detected (examples of such processes are shown in Fig.12). This selection, however, strongly reduces the relative magnitude of the polariton oscillations. A further reduction comes from the fact that the energy and momentum dissipation destroys the interference between the polaritons created at different points in the sample. In other words, a luminescent exciton interferes only ‘with itself’. It is surprising that even in this case the quantum polariton oscillations are not entirely suppressed and can be detected.

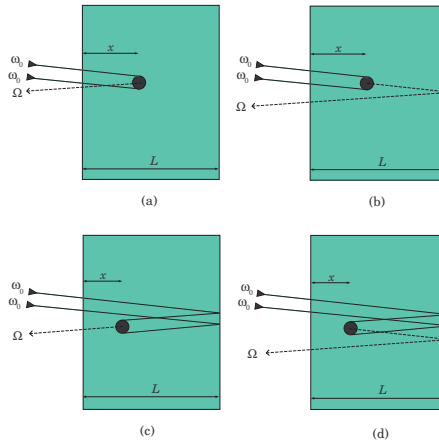


FIG. 12: Examples of nonlinear processes, in which two photons with frequency  $\omega_0$  are converted into a polariton with frequency  $\Omega$ . For clarity, the directions of propagation of the incident and emitted light are drawn slightly non-parallel.

In our simple model the intensity of the emitted light can be calculated as follows. Using the semiclassical method discussed above, we first find the radiation from the polaritons created at a point with the coordinate  $x$  in the sample. Then this intensity is multiplied by the conversion probability, weighted with a factor describing the absorption of the incident light in the sample, and integrated over  $x$  from 0 to  $L$ .

Consider, e.g., the process shown in Fig. 12a, in which two incident photons with frequency  $\omega_0$  enter the sample (with the probability  $(1 - R)^4$ ), the polariton travels along the path of length  $x$  in the direction opposite to that of the incident light, which gives the factor  $F^2(x, t)$  [cf. Eq.(20)], and then leaves the sample (the corresponding probability is  $(1 + R)^2$ ). For simplicity we assume the dielectric function for  $f = 0$  to be frequency independent, so that the reflection of both incident and emitted photons is described by the same coefficient  $R$ . The intensity of this process is then given by

$$I_a \propto (1 - R)^4 (1 + R)^2 \int_0^L dx e^{-2\alpha(\omega_0)x} F^2(x, t). \quad (22)$$

Here the factor  $e^{-2\alpha(\omega_0)x}$  describes the suppression of the intensity of the incident light squared ( $\alpha(\omega_0) \approx \frac{\omega_0}{\Omega} \alpha(\Omega)$ ). Actually, the time of the polariton motion is somewhat shorter than the total time  $t$  between the moments light enters and leaves the sample. However, the conversion is, by assumption, fast and the time of motion of the incident photons in the sample of thickness  $L = 0.3\text{mm}$ , used in this experiment, is only a few picoseconds, whereas the oscillation period is of the order of one nanosecond.

In the process shown in Fig. 12b, the polariton continues to move in the direction of the incident light and is reflected from the right boundary before leaving the sample (the path length is  $2L - x$ ). The reflection results in the

extra factor  $R^2$ :

$$I_b \propto (1 - R)^4 R^2 (1 + R)^2 \int_0^L dx e^{-2\alpha(\omega_0)x} F^2(2L - x, t). \quad (23)$$

Similarly, the sum of the intensities of the processes shown in Fig. 12c and d is

$$I_c + I_d \propto (1 - R)^4 R^4 (1 + R)^2 \int_0^L dx e^{-2\alpha(\omega_0)(2L-x)} [F^2(x, t) + R^2 F^2(2L - x, t)]. \quad (24)$$

In the same way one can find the emission intensity for the processes with multiple internal reflections of the incident and emitted photons.

This simple approach gives a reasonable description of the observed intensity oscillations, as shown in Fig. 6, where we plot the oscillating part of the intensity,  $I_{osc} = Ie^{\Gamma t}$ , measured experimentally (circles) and calculated theoretically. The dashed line is the sum of the contributions of all four types of processes depicted in Fig. 12 with multiple reflections included. We noted that the agreement with experiments improves, if the contributions of the processes shown in Fig. 12 a and d, in which the polariton is emitted in the direction opposite to that of incident light, are suppressed by the factor of 3. The rationale for doing this may be the fact that not all polaritons can reach the detector, since some of them are absorbed in the regions with dense exciton gas. Therefore, each of the processes discussed above has to be multiplied by a geometrical factor equal the fraction of excitons that can be detected. We did not perform the extensive calculations of this factor, since the results shown in Fig. 6 clearly show that the intensity oscillations result from the polariton beatings.

## VII. CONCLUSION

In conclusion, the here presented B-TPE process provides an efficient method to create a high density, cold exciton gas in the bulk of cuprous oxide. The low initial temperature of the gas (despite the energy mismatch), the instantaneous observation of  $X_{ortho}$  luminescence, and the preferential occupation of the  $k \approx 0$  state seem to point to a coherent type of B-TPE process as opposed to simple two photon absorption, and subsequent incoherent decay to the ortho exciton state. One possible process which would at least explain the low initial gas temperature would be two photon absorption from the upper valence band ( $+\Gamma_7$ ) that excites a continuum of excitonic  $p$  states associated with the upper conduction band ( $-\Gamma_8$ ).<sup>22</sup> Due to the spin selection rules the excitons created this way will be triplet excitons. However the  $C_2$  band originates from  $p$  orbitals so we do not have pure spin states for the electron anymore. Therefore the angular momentum selection rules allow the  $C_2$  triplet exciton to decay radiatively (dipole allowed transition) to either triplet or singlet  $C_1$  exciton and this way both para and ortho states of a yellow series may be populated. This could actually even happen in a coherent process (hyper-Raman scattering), with the V1-C2 electron-hole pair as the intermediate state. The details of the B-TPE process remain unclear at the present. Future experiments on photon emission coming from the C2-C1 transition should yield the necessary information.

We gave simple analytical expressions for the polariton oscillations observed both in the transmitted light in case of the resonant excitation and in the emitted light in time resolved two photon experiment. While in the first case the result is obtained by a straightforward application of the semiclassical method, the description of the beating that originates from a non-linear process requires additional assumptions. Since we have not found any evidence for the coherent production of the ortho-excitons, we assumed that the coherence of the incident light is lost in the irreversible conversion of two photons into a low-energy exciton. We argue that this does not completely suppress the polariton oscillations, since some polaritons can avoid the areas of dense exciton gas on their way to detector and live long enough to be considered as free particles. After such polaritons are created, they propagate as quantum superpositions of two polaritons, which gives rise to quantum beating, similar to the strangeness oscillations in K-mesons produced in hadron reactions [A. Angelopoulos *et al.*, Phys. Lett. B **503**, 49 (2001).] The shape of the oscillating intensity of light obtained within this simple approach is in good agreement with the experimental data.

Although the present study shows that ortho-exciton BEC can not be achieved in this kind of experiments, mainly because the particle decay rate is faster than the temperature decay, the TPE method does provide an efficient method to create a cold exciton gas. In particular, it allows to create a para-exciton gas in conditions where ortho-para down-conversion is blocked (*i.e.* at low temperatures), opening new possibilities in the excitonic BEC quest.

*Acknowledgments.* The authors acknowledge fruitful discussions with D. van der Marel. This work was supported by the Stichting voor Fundamenteel Onderzoek der Materie (FOM, financially supported by the Nederlandse

- \* Present address: Institute of Physics, Polish Academy of Sciences, 02 668 Warsaw, Poland. e-mail: karpik@ifpan.edu.pl  
† Electronic address: p.h.m.van.loosdrecht@rug.nl
- <sup>1</sup> S. A. Moskalenko and D. W. Snoke, *Bose-Einstein Condensation of Excitons* (Cambridge University Press, Cambridge, 2000).
  - <sup>2</sup> A. Griffin, D. W. Snoke, and S. Stringari, eds., *Bose-Einstein Condensation* (Cambridge University Press, Cambridge, 1995).
  - <sup>3</sup> D. W. Snoke and V. Negoita, *Phys. Rev. B* **61**, 2904 (2000).
  - <sup>4</sup> C. W. Lai, J. Zoch, A. C. Gossard, and D. S. Chemla, *Science* **303**, 503 (2004).
  - <sup>5</sup> D. W. Snoke, Y. Liu, S. Denev, L. Pfeiffer, and K. West, *Solid State Comm.* **127**, 187 (2003).
  - <sup>6</sup> D. W. Snoke, D. Braun, and M. Cardona, *Phys. Rev. B* **44**, 2991 (1991).
  - <sup>7</sup> N. Naka and N. Nagasawa, *Phys. Rev. B* **65**, 075209 (2002).
  - <sup>8</sup> N. Naka and N. Nagasawa, *Phys. Rev. B* **70**, 155205 (2004).
  - <sup>9</sup> M. Kubouchi, K. Yoshioka, R. Shimano, A. Mysyrowicz, and M. Kuwata-Gonokami, *Phys. Rev. Lett.* **94**, 016403 (2005).
  - <sup>10</sup> D. Fröhlich, A. Kulik, B. Uebbing, V. Langer, H. Stolz, and W. von der Osten, *Phys. Stat. Sol. (b)* **173**, 31 (1992).
  - <sup>11</sup> D. Fröhlich, A. Kulik, and B. Uebbing, *Phys. Rev. Lett.* **67**, 2343 (1991).
  - <sup>12</sup> D. W. Snoke, J. P. Wolfe, and A. Mysyrowicz, *Phys. Rev. Lett.* **59**, 827 (1987).
  - <sup>13</sup> E. Ruiz, S. Alvarez, P. Alemany, and R. A. Evarestov, *Phys. Rev. B* **56**, 7189 (1997).
  - <sup>14</sup> K. E. O'Hara and J. P. Wolfe, *Phys. Rev. B* **62**, 12909 (2000).
  - <sup>15</sup> S. Denev and D. W. Snoke, *Phys. Rev. B* **65**, 085211 (2002).
  - <sup>16</sup> C. K. Teh and F. L. Weichman, *Can. J. Phys.* **61**, 1423 (1983).
  - <sup>17</sup> R. D. Schmidt-Withley, M. Martinez-Clemente, and A. Revcolevschi, *J. Crystal Growth* **23**, 113 (1974).
  - <sup>18</sup> T. Ohyama, T. Ogawa, and H. Nakata, *Phys. Rev. B* **56**, 3871 (1997).
  - <sup>19</sup> K. Karpinska, P. van Loosdrecht, I. Handayani, and A. Revcolevschi, *J. Lumin.* **112**, 17 (2005).
  - <sup>20</sup> I. S. Gorban, V. O. Gubanov, I. M. Dmitruk, and V. D. Kulakovskii, *J. Luminescence* **87-89**, 222 (2000).
  - <sup>21</sup> T. Ito and T. Masumi, *J. Phys. Soc. Jpn.* **66**, 2185 (1997).
  - <sup>22</sup> K. C. Rustagi, F. Padere, and A. Mysyrowicz, *Phys. Rev. B* **8**, 2721 (1973).
  - <sup>23</sup> G. M. Kavoulakis, *Phys. Rev. B* **61**, 035204 (2002).
  - <sup>24</sup> Y. Sun, K. Rivkin, J. Chen, J. B. Ketterson, P. Markworth, and R. P. Chang, *Phys. Rev. B* **66**, 245315 (2002).
  - <sup>25</sup> Y. C. Lee and W. Zhu, *J. Phys.: Condensed Matter* **12**, L49 (2000).
  - <sup>26</sup> C. Ell, A. Ivanov, and H. Haug, *Phys. Rev. B* **57**, 9663 (1998).
  - <sup>27</sup> H. Haug, *Journal of Lumin* **69**, 83 (1999).
  - <sup>28</sup> N. Mott and H. Massey, *Theory of Atomic Collisions* (Clarendon, Oxford, 1965).